Journal of Occupational and Environmental Hygiene
Publication details, including instructions for authors and subscription information:
http://www.informaworld.com/smpp/title~content=t713657996

On the Inconsistencies Related to Prediction of Flow into an Enclosing Hood Obstructed by a Worker

Ertan Karaismail[a]; Ismail Celik[a]
[a] Mechanical and Aerospace Engineering Department, West Virginia University, Morgantown, West Virginia

First published on: 30 March 2010

To cite this Article Karaismail, Ertan and Celik, Ismail(2010) 'On the Inconsistencies Related to Prediction of Flow into an Enclosing Hood Obstructed by a Worker', Journal of Occupational and Environmental Hygiene, 7: 6, 315 — 325, First published on: 30 March 2010 (iFirst)
To link to this Article: DOI: 10.1080/15459621003717854
URL: http://dx.doi.org/10.1080/15459621003717854

Journal of Occupational and Environmental Hygiene, 7: 315–325
ISSN: 1545-9624 print / 1545-9632 online

DOI: 10.1080/15459621003717854

On the Inconsistencies Related to Prediction of Flow into an Enclosing Hood Obstructed by a Worker

Ertan Karaismail and Ismail Celik

Mechanical and Aerospace Engineering Department, West Virginia University, Morgantown, West Virginia

The recirculating flow structures formed in the wake of a worker standing in front of an enclosing fume hood were numerically investigated. Two- and three-dimensional, unsteady, laminar/turbulent computations were performed for a Reynolds number (Re) range of $1.0 \times 10^3 - 1.0 \times 10^5$. The standard $k-\varepsilon$, Renormalization group (RNG) $k-\varepsilon$, and Shear Stress Transport (SST) $k-\omega$ models were used in Unsteady Reynolds Averaged Navier-Stokes (URANS) computations, and the results were compared with each other and also with the previous predictions reported in the literature. Numerical issues regarding the grid convergence and the inadequacies of turbulence models that may come into play at low Reynolds numbers were addressed. On the whole, SST $k-\omega$ model was found to be promising for qualitatively accurate prediction of both steady and unsteady recirculatory flow patterns in the wake of the worker. On the other hand, the standard and RNG $k-\varepsilon$ models failed in prediction of anticipated unsteadiness at low Reynolds numbers. In a more realistic three-dimensional simulation with SST $k-\omega$ model, the anticipated unsteady and recirculating flow field in the wake of the worker was captured. Present results seem to qualitatively agree with the deductions made from experimental analyses in the literature while conflicting with some aspects of the previously reported numerical results. The apparent inconsistencies observed between the current results and those published in the literature were elucidated.

Keywords enclosing fume hoods, turbulent flows, wake flows

Address correspondence to: Ertan Karaismail, Mechanical and Aerospace Engineering Department, West Virginia University, Morgantown, WV 26506-6106; e-mail: ekaraism@mix.wvu.edu.

INTRODUCTION

In industry, bench-top enclosing fume hoods, without sash, are widely used to protect workers from potentially hazardous materials that may become airborne while performing routine procedures. Recently, transport of these airborne contaminants inside and around the hoods has received considerable research interest due to increasing concerns with fugitive emission and worker exposure.

Understanding the flow dynamics in the wake of a worker standing against a fume hood is of great importance from the standpoint of reducing the exposure level. The flow under consideration can be classified as an accelerating/converging flow past a bluff body, since the worker's torso acts as an obstacle to the flow drawn into the hood. Following the previous studies,[1–3] in two-dimensional simulations, the worker is represented with an ellipse positioned in front of a contraction representing the hood. Practically, in such flows, typical Reynolds numbers, based on the airflow velocity (0.05 – 5 m/s) and the half of the worker's shoulder diameter (0.3 – 0.6 m) are in the range of $1.0 \times 10^3 - 1.0 \times 10^5$.[1] In the absence of contraction, for this range of Reynolds number, the flow regime around the worker, when it is represented as an elliptical cylinder with an aspect ratio of 0.5, encompasses the subcritical flow regime[4] with characteristic features of separation and vortex shedding. On the other hand, the flow inside the fume hood is exclusively characterized as turbulent. Furthermore, the turbulence and vortices formed in the wake can be suppressed by the re-laminarization effect of acceleration due to convergence of the flow into the hood (contraction). Indeed, a combination of all the aforementioned flow features is anticipated to take place simultaneously, in real situations.

In the literature, there are a number of experimental investigations[5–9] related to worker exposure and enclosing fume hoods. From these studies conforming the theory, it has become clear that the contaminants released in a fume hood can be dispersed outward due to periodic or unstable vortices or by large scale turbulence in an unstable wake region in front of a worker. On the other hand, much of the effort in numerical studies on worker exposure has been devoted to flows past bluff bodies, such as elliptical or circular cylinders, immersed in a free-stream,[2,10–14] and the findings from these studies are of limited use for the case in question, due to dramatic change of flow regime caused by the presence of hood/contraction and suction into the hood.

Nevertheless, a limited number of numerical studies relevant to enclosing hoods with a bluff body or worker obstruction[1,15–18] have been reported in the literature. Interestingly, while experimental studies and theory indicate formation of worker-induced recirculating flow structures, these numerical analysis, except for Chern and Cheng,[15]

reported that no or negligibly small recirculation zones are present in the wake. Indeed, in Chern and Cheng, the worker is represented as a rectangular block body, which is more prone to cause flow separation leading to formation of vortices in the near wake of the worker. Aside from the fact that the investigated hood is a laboratory type with a sash, it is not very clear from the publication whether the reported vortices are induced by the flow separation around the worker or at the edge of bottom plate of hood.

Although it is a difficult task to achieve quantitative accuracy in prediction of the complex flow phenomena around bluff bodies, a qualitatively reliable prediction of the flow features could provide useful insight into the contaminant transport in the wake of the worker. The observed inconsistencies, even qualitatively, between the numerical predictions and the experimental findings can be attributed to the differences in the cases (e.g., hood types, suction rates) investigated, and to the numerical factors such as discretization schemes, grid resolutions, and different approaches to turbulence modeling. However, one of the common aspects of the reviewed numerical studies was the exclusive employment of the standard $k-\varepsilon$ turbulence model[19] in conjunction with the standard wall function formulation. This approach allows the use of a relatively coarse grid in the near-wall region and assumes equilibrium between the turbulent production and dissipation. However, it is only valid for high Reynolds number and fully turbulent core flows and is expected to be inadequate in flows where pervasive low Reynolds number and near-wall effects are predominant and when strong adverse pressure gradient leads to boundary layer separation (*FLUENT 6.3 User Manual*; ANSYS Inc., Canonsburg, Pa.). In addition to this, the isotropic eddy viscosity concept, on which the standard $k-\varepsilon$ turbulence model is based, is known to produce unrealistically high turbulent kinetic energy (k) upstream of the bluff body that causes late separation and subsequent suppression of the near wake.[20,21] Therefore, the suitability of the standard $k-\varepsilon$ turbulence model in conjunction with the standard wall function formulation is dubious and may point to further investigation.

A more suitable approach that can capture the important flow structures for the flow under consideration is the Large Eddy Simulation (LES). However, despite the growing applicability of LES with increasing computational capabilities, it still requires considerable, sometimes prohibitive, computational resources for large-scale industrial problems. Therefore, Reynolds Averaged Navier-Stokes (RANS) modeling that offers comparatively less computational cost is expected to be in use for a long time. With proper application of RANS modeling, fast and reasonably accurate predictions can be made for many industrial problems.

Taking into consideration the aforementioned features of the flow, the authors believe that using an appropriate turbulence model along with a proper near-wall treatment and grid resolution are of key importance in terms of reliable prediction of the physics encompassed in the flow considered, especially in the wake of the worker. In light of such background, and the motivation to resolve the inconsistent findings in the literature, the aims of this study are (1) to test the performances of different turbulence models and wall treatments by comparing the results with the previously reported findings, (2) to recommend a promising RANS turbulence model for future analysis, (3) to make the industrial hygiene community aware of the numerical complications that may come into picture in numerical simulations, and (4) to shed some light on the flow patterns in a realistic three-dimensional flow. To this end, the standard $k-\varepsilon$, RNG $k-\varepsilon$[22] and SST $k-\omega$[23] turbulence models were chosen and calculations were carried out for two- and three-dimensional test cases. Due to lack of experimental data, the focus of this study is primarily on the qualitative predictability of the anticipated recirculation zone and the unsteadiness arising from the onset of vortex shedding in the wake region.

DESCRIPTION OF TEST CASES

Two-Dimensional Case

The two-dimensional test case adopted in this study is a simple conceptual model (Figure 1) originally presented by Dunnett.[1] Simulations were run for Reynolds numbers in the range of $1.0 \times 10^3 - 1.0 \times 10^5$ to investigate the two-dimensional wake flow of an ellipse representing the worker. In this flow configuration, the center of the ellipse is $0.75a$ away from the face of the exhaust opening, representing a hood, as shown in Figure 1. Although this two-dimensional analysis is a crude approximation of a real situation (as already pointed out by Dunnett), George et al.[13] found in an experimental work that a two-dimensional approach may provide a reasonable approximation to the physics of the problem. To conform with Dunnett's study, Reynolds number is defined as $\mathrm{Re} = aU_0/2\nu_{\mathrm{air}}$ based on the inlet velocity (U_0), kinematic viscosity of air (ν_{air}) and the half of the major axis dimension ($a/2$) of the ellipse. The major axis dimension of the ellipse (a) and the air velocity (U_0) were set to 0.6 m and 5 m/s, respectively, so that the Reynolds number is c.a. 1.0×10^5, which is used by Dunnett. Again, in accordance with Dunnett's work, a time step (Δt) of 6.0×10^{-3} sec was used in the simulations.

To match the boundary conditions used by Dunnett,[1] at the inlet and outlet of the solution domain, velocity boundary conditions satisfying the mass conservation were imposed. This led to an inlet velocity (U_0) of 5m/s. The free-stream turbulence intensity was taken as 10% of the inlet velocity (U_0), which is also the same as in Dunnett. At the inlet and outlet, conforming to Dunnett's settings, turbulent kinetic energy (k) and dissipation rate (ε) were calculated from $k = 0.005U_0^2$ and $\varepsilon = k^{3/2}/0.15a$, respectively. For the SST $k-\omega$ model computations, specific dissipation rate (ω) was calculated from ε/kC_μ, where C_μ is an empirical constant equal to 0.09. No slip boundary conditions were used for all of the walls. For other cases ($\mathrm{Re} = 1.0 \times 10^4$ and $\mathrm{Re} = 1.0 \times 10^3$), the inlet velocity was adjusted to attain the desired Reynolds number.

In an attempt to repeat Dunnett's calculations,[1] first, simulations with the standard $k-\varepsilon$ turbulence model were run

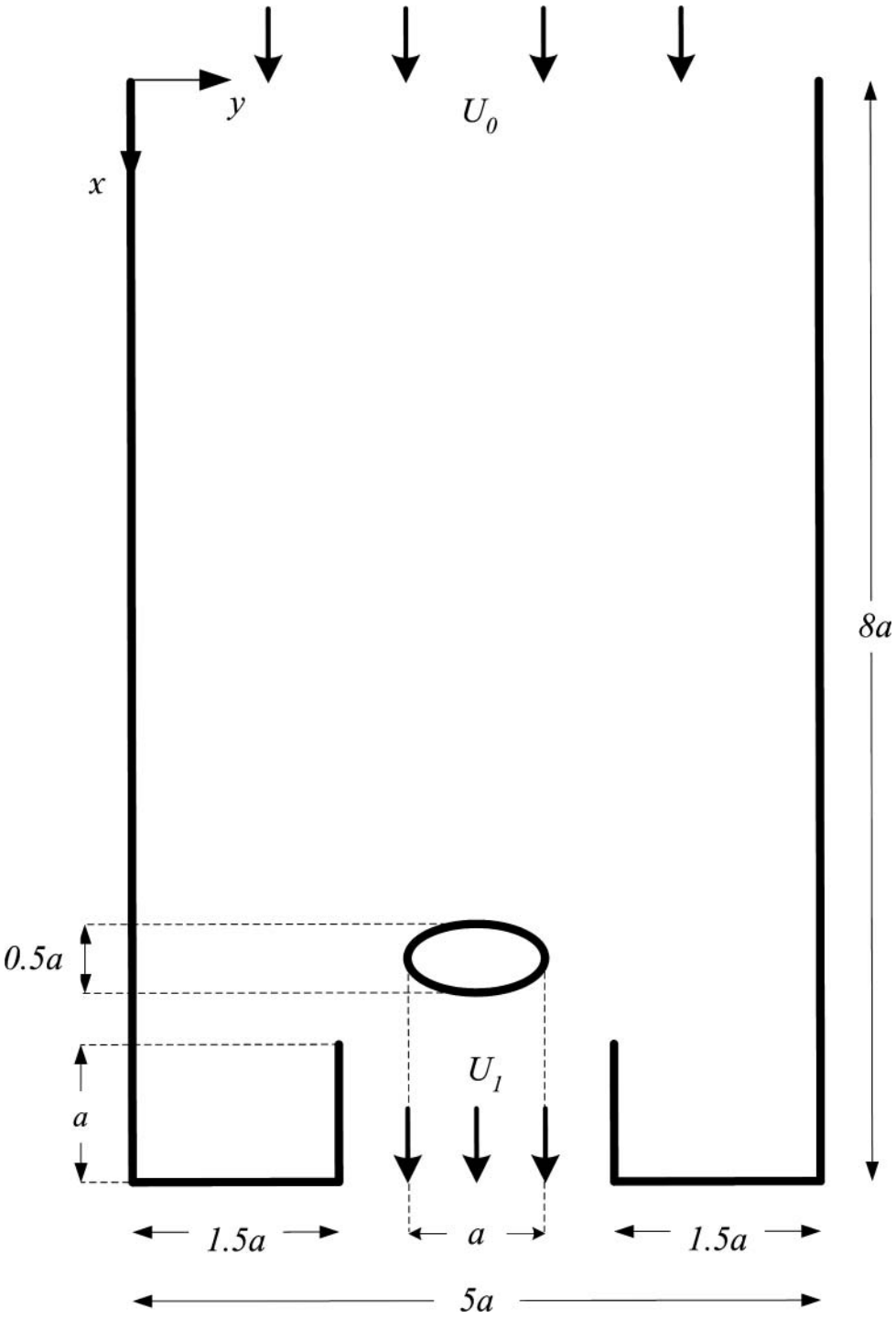

FIGURE 1. Schematic representation of the flow configuration.

on meshes with different resolutions, and grid convergence is investigated at this Reynolds number (1.0×10^5). Then, the same calculations were performed on the same grids for an improved type of $k - \varepsilon$ family of turbulence models, namely, RNG $k - \varepsilon$ model, and SST $k - \omega$ turbulence model; the latter is considered to be more accurate and reliable for a wide range class of flows including adverse pressure gradient flows.[24] Although successively finer grids were used for grid convergence analysis, focus was placed principally on the level of grid resolution in the near-wall region because the location of separation and, therefore, the size of the recirculation zone, are affected mainly by the grid resolution in this region.

On the whole, seven different grids becoming denser around the ellipse were generated with GAMBIT software included

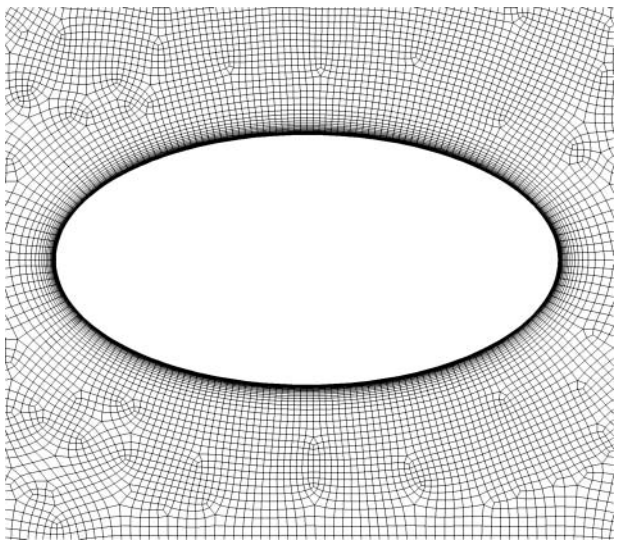

FIGURE 2. Detail view of grid (G6) around the ellipse (for Re = 1.0×10^5).

in FLUENT 6.3 (ANSYS Inc.) commercial computational fluid dynamics (CFD) package. Two-dimensional structured boundary layer grids extending c.a. 10–15% of the major axis of the ellipse were generated to control the spacing of the first interior grid point away from the ellipse (Δy_1). The rest of the domain was meshed with Quad/Pave scheme, which leads to non-orthogonal rectangular cells. The consequent grid structure around the ellipse is shown in Figure 2. On the whole, the grids generated differ in number of total cells as well as in spacing of the first interior grid (Δy_1). The details of the grids used are listed in Table I.

In the calculations, standard wall functions were used if the average y^+(first interior grid in wall distance units) is greater than 30; otherwise, the enhanced wall treatment approach was used. The enhanced wall treatment method combines a two-layer model with enhanced wall functions and becomes identical to the two-layer zonal method when $y^+ \sim 1$ (G7). On the other hand, provided that the grid resolution is high enough, ($y^+ \sim 1$) SST $k - \omega$ model does not need any wall functions in the near-wall regions and, therefore, is integrated down to the wall without using any damping functions.

The effect of grid refinement on prediction of the angle of separation, θ_s (location where axial wall shear stress is zero on the surface of the ellipse), as measured clockwise from the upstream stagnation point, and the length of recirculation zone, X_r (distance between the location of confluence point and the downstream stagnation point of the ellipse) is illustrated in Figure 3. From Figure 3A, it can be seen that, in general, the angle of separation decreases (location of separation moves upstream) with increasing grid resolution in the near-field. Interestingly, for large values of Δy_1 (from 1.8×10^{-3} to 7.2×10^{-3}m) RNG $k - \varepsilon$ and SST $k - \omega$ model predictions collapse on the same curve. However, the same agreement is not seen in the convergence of the recirculation zone length (Figure 3B). Further discussion on separation angle and recirculation zone length can be found in the Results and Discussion section.

Assuming the most reliable solutions are obtained on a fully resolved grid ($y^+ \sim 1$), the behaviors of the solutions at moderate and low Reynolds number (1.0×10^4 and 1.0×10^3, respectively) were tested on a mesh fine enough to resolve the near-wall region.

Three-Dimensional Case

Three-dimensional case is a realization of the airflow into an industrial type enclosing fume hood (without sash) obstructed by a worker located in a wind tunnel measuring 4.92 × 2.74 × 3.66 m^3 (*depth* × *height* × *width*). The hood is 0.91 × 0.76 × 1.14 m^3 and has a plenum section at the end to adjust the pressure distribution for a more uniform flow field inside the hood. The 1.68-m-tall worker is approximated as a rounded body consisting of anthropometrically scaled sphere, an elliptical cylinder, and two circular cylinders representing the head, torso, and legs, respectively.

The computational domain begins 5 shoulder diameters ($D_s \sim 0.45$ m) upstream of the hood. A non-uniform, conformal, hybrid (structured/unstructured) mesh containing about 1,472,000 tetra- and hexa-hedral cells was employed. Finer cells were used around the manikin and inside the hood to enable capture of the coherent flow structures. The

TABLE I. Number of Cells Used in Two-Dimensional Simulations

Grid	Re = 1.0×10^5	Re = 1.0×10^4	Re = 1.0×10^3
G1	9594 ($\Delta y_1 = 7.2 \times 10^{-3}$m)	51,144[B] ($\Delta y_1 = 4.6 \times 10^{-4}$m)	51,144[B] ($\Delta y_1 = 4.6 \times 10^{-4}$m)
G2	24,993 ($\Delta y_1 = 3.6 \times 10^{-3}$m)		
G3	49,037 ($\Delta y_1 = 2.7 \times 10^{-3}$m)		
G4	59,340[A] ($\Delta y_1 = 1.8 \times 10^{-3}$m)		
G5	76,663[A] ($\Delta y_1 = 9.0 \times 10^{-4}$m)		
G6	81,081[A] ($\Delta y_1 = 1.8 \times 10^{-4}$m)		
G7	93,883[A] ($\Delta y_1 = 6.0 \times 10^{-5}$m)		

[A]Enhanced wall treatment was used in $k - \varepsilon$ model calculations.
[B]Transitional flow modifications were enabled in SST $k - \omega$ model calculations.

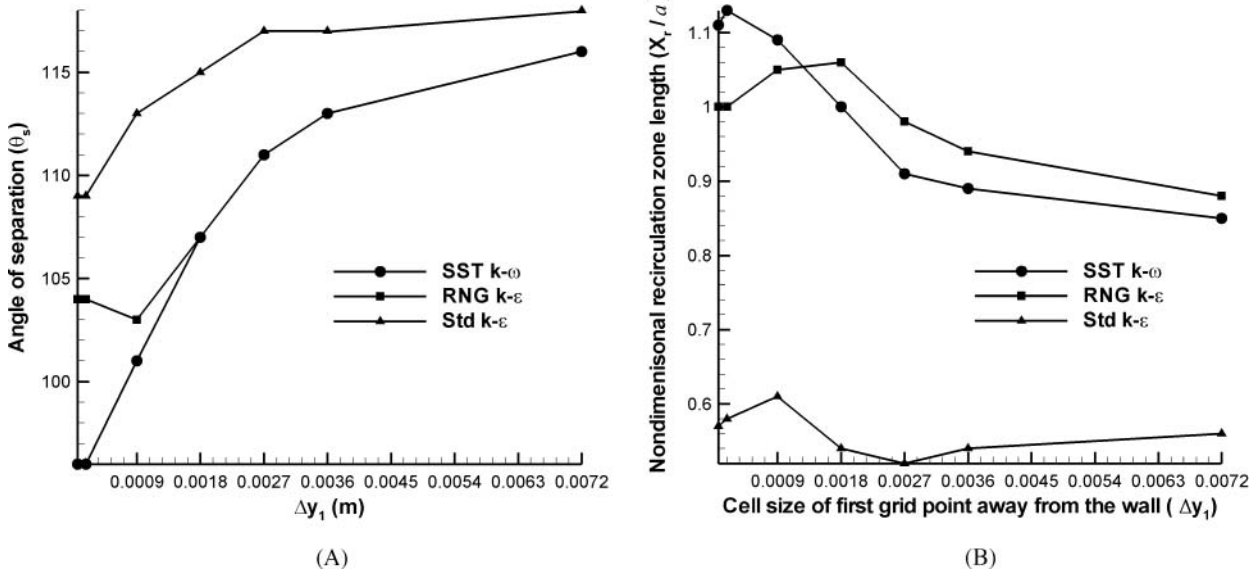

FIGURE 3. Variation of (A) angle of separation (measured from upstream stagnation point); (B) nondimensional recirculation zone length ($a = 0.6$m), with (Δy_1).

computational geometry and the grid structure in the region of interest are illustrated in Figure 4.

The SST $k - \omega$ turbulence model, which was found to be more suitable and reliable from two-dimensional test case, is used in these computations. The Reynolds number is c.a. 3.0×10^3 based on the half of the larger diameter of the elliptic torso and the free-stream velocity (0.2 m/s). At the inlet of the wind tunnel, a uniform velocity of 0.2 m/s along with a turbulent intensity of 10% and a turbulent viscosity ratio of 10 were specified. Similarly, at the duct exit a uniform velocity of 9.56 m/s with 10% turbulent intensity and a turbulent viscosity ratio of 10 were defined. At the wind tunnel outlet, an outflow boundary condition that assumes zero normal gradients for all flow variables, except for the pressure, was imposed. No-slip boundary conditions were imposed at all solid walls, such as wind tunnel walls, hood walls, and worker.

The effects of the walls were computed by the enhanced wall treatment that applies standard wall function when the

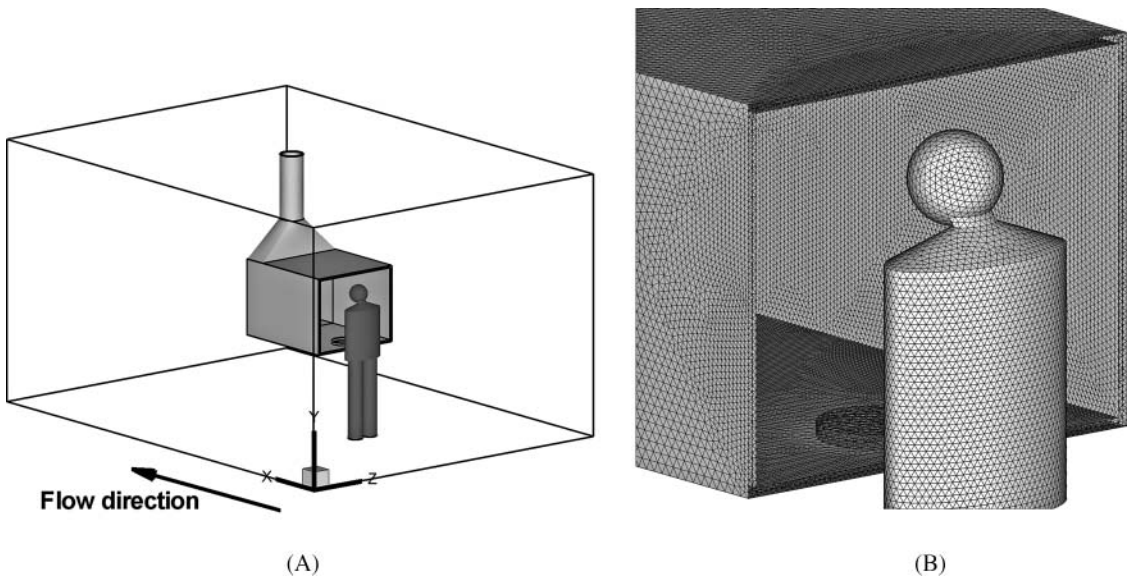

FIGURE 4. Representation of (A) computational domain, (B) mesh around the hood and the worker.

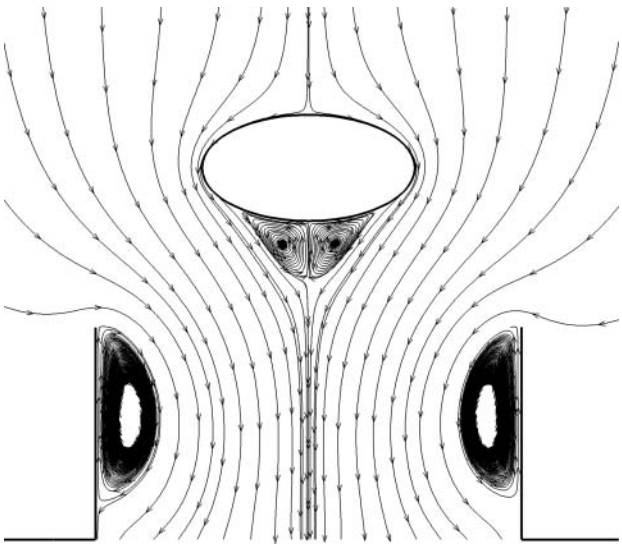

FIGURE 5. Stream-traces predicted on coarse grid (G1) with the standard k-ε turbulence model at Re = 1.0×10^5.

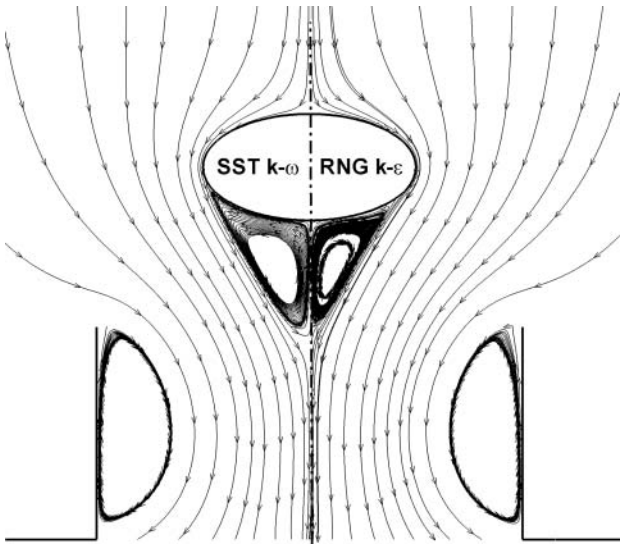

FIGURE 6. Comparison of the stream-traces predicted by fully resolved (G7) SST k-ω and RNG k-ε turbulence models at Re = 1.0×10^5.

mesh is coarse; otherwise, it switches to the appropriate low Reynolds number boundary conditions (enhanced wall functions). In the present calculations, the average value of y^+ around the worker is less than 10, ensuring the use of enhanced wall functions around the worker. The plenum section was modeled by a porous jump boundary condition. A time step (Δt) of 1.0×10^{-3} seconds was used for time marching.

NUMERICAL METHOD

The commercial CFD software FLUENT 6.3 (ANSYS Inc.) was used to solve two/three-dimensional, Navier-Stokes (NS) and URANS equations with the Finite Volume Method (FVM) on a collocated grid. The Quadratic Upwind Interpolation (QUICK) scheme was used for spatial discretization of convective terms in the momentum equation, whereas second-order upwind scheme was used for discretization of all other convective terms in other transport equations. All diffusive terms were discretized by second order central differencing scheme. A first-order-accurate unconditionally stable implicit scheme was used for time discretization. SIMPLEC algorithm was used for velocity-pressure coupling. Sufficient convergence at each time step was assumed to be reached when the sum of the scaled residuals is less than 1×10^{-4}. In cases where the flow exhibited unsteady behavior, simulations were run until a nearly periodic flow was observed to analyze the frequency response of the flow.

RESULTS AND DISCUSSION

Two-Dimensional Case

For the high Reynolds number case (Re = 1.0×10^5), the stream-traces in the near-field of the ellipse predicted by the standard $k - \varepsilon$ turbulence model calculations on the coarsest grid (G1) are shown in Figure 5, where it is clear that even with the standard wall functions, the standard $k-\varepsilon$ turbulence model captures boundary layer separation leading to a steady and symmetric recirculation zone in the wake of the ellipse. For the same conditions, these vortex pairs developed in the wake were not captured in Dunnett's[1] simulations. The possible reasons for this disagreement might be the differences in quality and resolution of the grid around the ellipse or implementation of the turbulence model. The recirculation zones attached to the hood walls are due to separation of the incoming flow, especially from the sides, at the hood walls. These recirculation zones can also be seen in Dunnett's predictions.

From Figure 3, shown in the description of two-dimensional case, it is seen that the length of the recirculation zone is correlated with the location of separation, as θ_s decreases toward 90°, X_r increases, and vice versa. Furthermore, the predicted X_r values using the standard $k - \varepsilon$ model computations are remarkably smaller compared with those of RNG $k - \varepsilon$ and SST $k - \omega$ models. This situation may be attributed, in general, to a shortcoming of the standard $k - \varepsilon$ models, whereby they produce high levels of turbulent viscosity and, hence, suppress the vortices. This issue is examined further for moderate Reynolds number (1×10^4) in more detail.

Figure 6 depicts to what extent the predicted recirculation zones extend toward the hood. It is observed that for the condition under consideration, the recirculation zone does not extend into the hood. If it extended into the hood, in practice, the contaminants might be carried to the breathing zone of the worker by the reverse flow. The recirculation zones predicted by both turbulence models are smaller than in cases without a hood (not shown). The convergence of the airflow into the hood suppresses the recirculation region and makes it narrower toward to hood entrance.

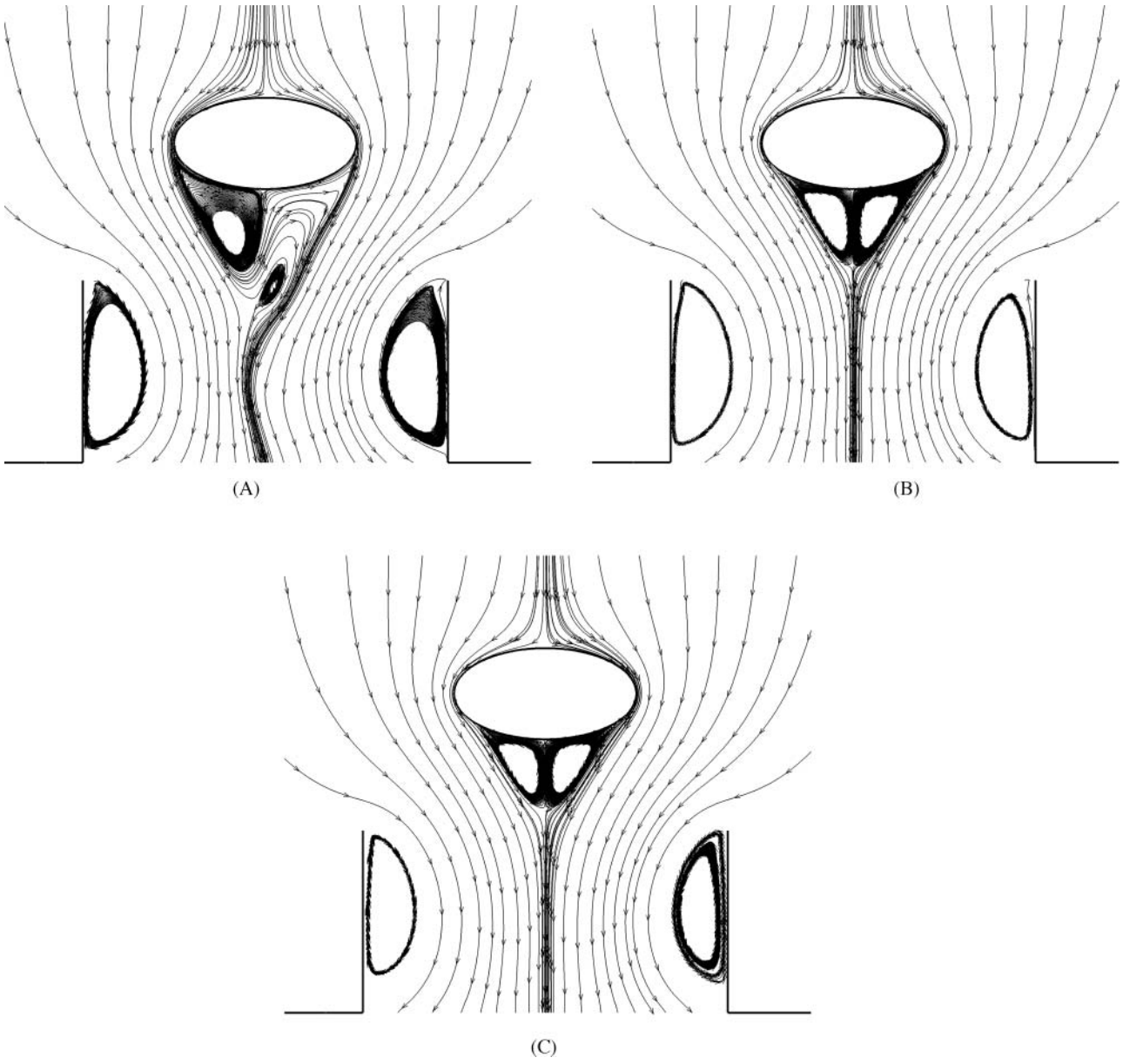

FIGURE 7. Predicted stream-traces at 4000 time step at $\mathrm{Re} = 1.0 \times 10^4$; (A) SST k-$\omega$ model, (B) RNG k-ε model, (C) standard k-ε model.

Figure 7 illustrates how the SST $k-\omega$ model predicts drastically different flow patterns compared with the $k-\varepsilon$ models at a moderate Reynolds number (1.0×10^4). Theoretically, at this Reynolds number, vortex shedding should be observed for a flow around an ellipse immersed in a free-stream.[4] However, the presence of hood (contraction) and, hence, the acceleration of the flow into the hood are expected to change the flow pattern downstream of the ellipse. From the SST $k-\omega$ model predictions shown in Figure 7A, the anticipated unsteadiness and asymmetry of the flow due to onset of vortex shedding can be clearly observed. However, the vortex shedding is suppressed due to convergence of the flow into the hood, and a pair of vortices attached to the ellipse undulates instead.

On the other hand, the standard and RNG $k-\varepsilon$ models, still predicted steady recirculation zones, as shown in Figures 7B and 7C. This result not only confirms the point made by Franke and Rodi[25]—on the failure of standard $k-\varepsilon$ turbulence model in predicting unsteady separated flows behind bluff bodies—but also extends it to RNG $k-\varepsilon$ model. In an attempt to understand why the $k-\varepsilon$ models fails to capture the unsteadiness, contours of the turbulent viscosities (μ_T) computed by all models are plotted in Figure 8. A closer look at the immediate proximity of the ellipse reveals that the standard and RNG $k-\varepsilon$ turbulence models lead to higher turbulent viscosities in this region, which, in turn, change the effective Reynolds number that can be defined as $Re^{\mathrm{eff}} = DU\rho/\mu^{\mathrm{eff}}$, where μ^{eff} is the summation of laminar

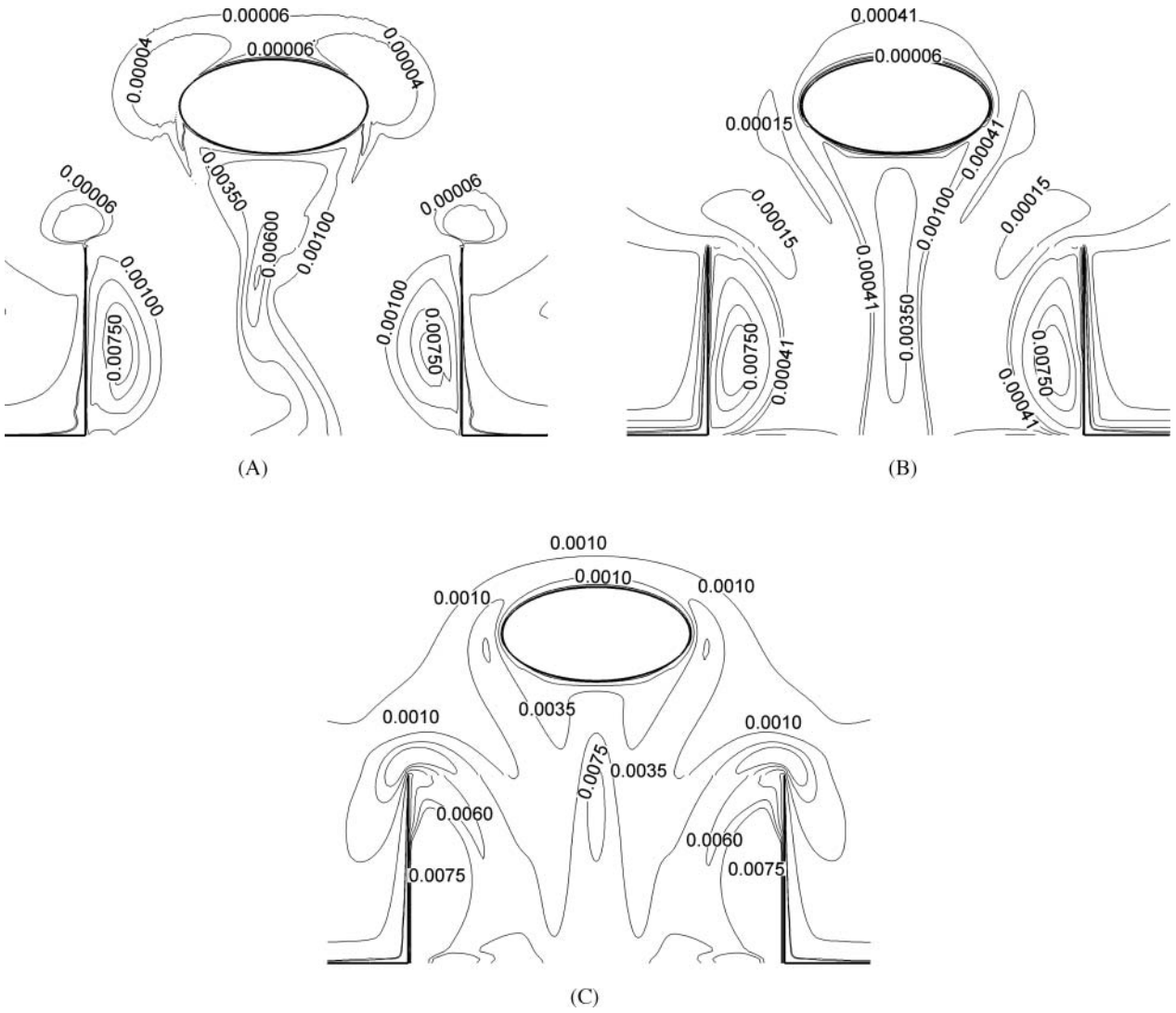

FIGURE 8. Calculated turbulent viscosities at 4000 time step at Re = 1.0×10^4; (A) SST k-ω model, (B) RNG k-ε model, (C) standard k-ε model.

and turbulent viscosities ($\mu^{\text{eff}} = \mu_L + \mu_T$). An increase in the effective viscosity (μ^{eff}) gives rise to a decrease in Re^{eff} and, hence, to a change in flow regime. Reducing the grid size substantially decreases the turbulent viscosity only slightly, which does not improve the predictions much. Assuming that the SST $k - \omega$ model predictions are more accurate, it can be concluded that the standard $k - \varepsilon$ turbulence model damps out the velocity variations around the ellipse, leading to a high degree of smoothing of the gradients in the flow.

The time history of the stream-wise velocity, from SST $k-\omega$ model computation, monitored at a point ($x = 2.4a$, $y = 6.57a$) in the wake, is presented in Figure 9A. The calculated power spectrum of the presented velocity oscillations is illustrated in Figure 9B. As can be seen from the figure, the frequency of the oscillations is 1.91 Hz, which corresponds to a Strouhal number (Sr) of 2.29 based on the dimension of the major axis of the ellipse ($a = 0.6$ m) and the free-stream velocity ($U_0 = 0.5$ m/s). These high frequency (Sr = 2.29) oscillations are due mainly to the effect of contraction that channels the flow toward the hood entrance, leading to an alternating confinement of the vortices from either side, immediate downstream of the ellipse. Therefore, the vortices do not have enough time to shed freely, as it happens in the absence of hood.

To ensure that this high Strouhal number is not due to the mesh resolutions, simulations in the absence of contraction were run on the same mesh, and a Strouhal number of 0.25 is obtained, which deviates slightly from the theoretical value of c.a. 0.2, reported for flows past ellipse immersed in a free-stream.[4] The blockage by the side walls present in the computational domain might have contributed to this slight deviation from the theoretical value.

At low Reynolds number (1.0×10^3), both laminar and SST $k - \omega$ model computations were performed. Theoretically,

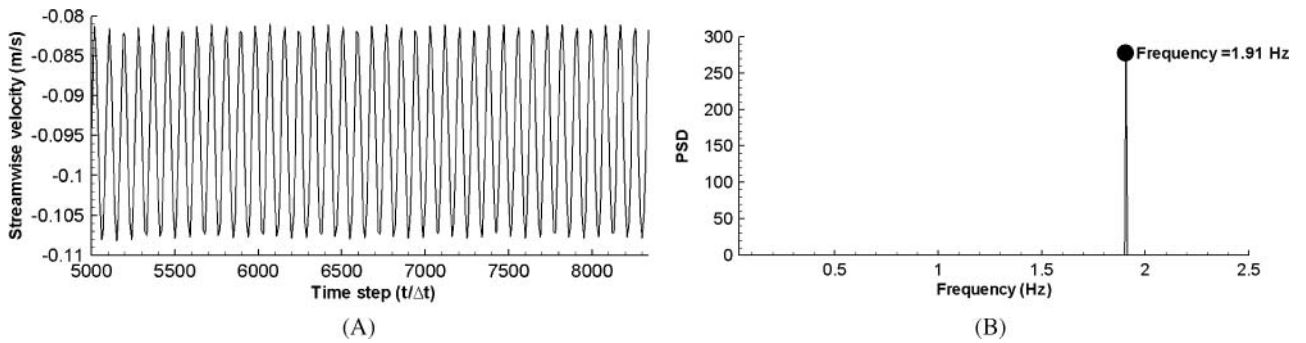

FIGURE 9. Stream-wise velocity from SST k-ω model at a point (x = 2.4a, y = 6.57a) at Re = 1.0 × 10^4; (A) time history, (B) power spectral density, PSD.

the asymmetry in the wake flow is expected to be more pronounced in the low Reynolds number case. The much stronger oscillations obtained from the laminar computations (Figures 10A and 10B) confirm this postulation. The dominant frequency (0.086Hz) of the velocity oscillations corresponds to a Strouhal number of 1.03.

On the other hand, SST $k-\omega$ model, which is considered to be suitable for low Reynolds number flows as well, captured the oscillatory behavior with a frequency of 0.176 Hz (Sr = 2.11) (Figures 10C and 10D). Although these oscillations are much weaker compared with the ones from laminar computations, they point to the fact that SST $k-\omega$ turbulence model can be used for transitional flows. These unsteady flow structures captured in the present laminar calculations are much more pronounced than those reported by Dunnett[1] for the case of Re = 1.0 × 10^3.

On the whole, the predictions indicated that depending on the suction rate by the hood, steady or unsteady recirculation zones can form in the wake of the worker. Because of the effect of converging flow, the sizes of these zones are limited to the spacing between the worker and the hood; so, for the given flow configuration, the reverse flow is not expected to carry the contaminants from the hood back to the breathing zone of the worker. However, it should be kept in mind that contaminants

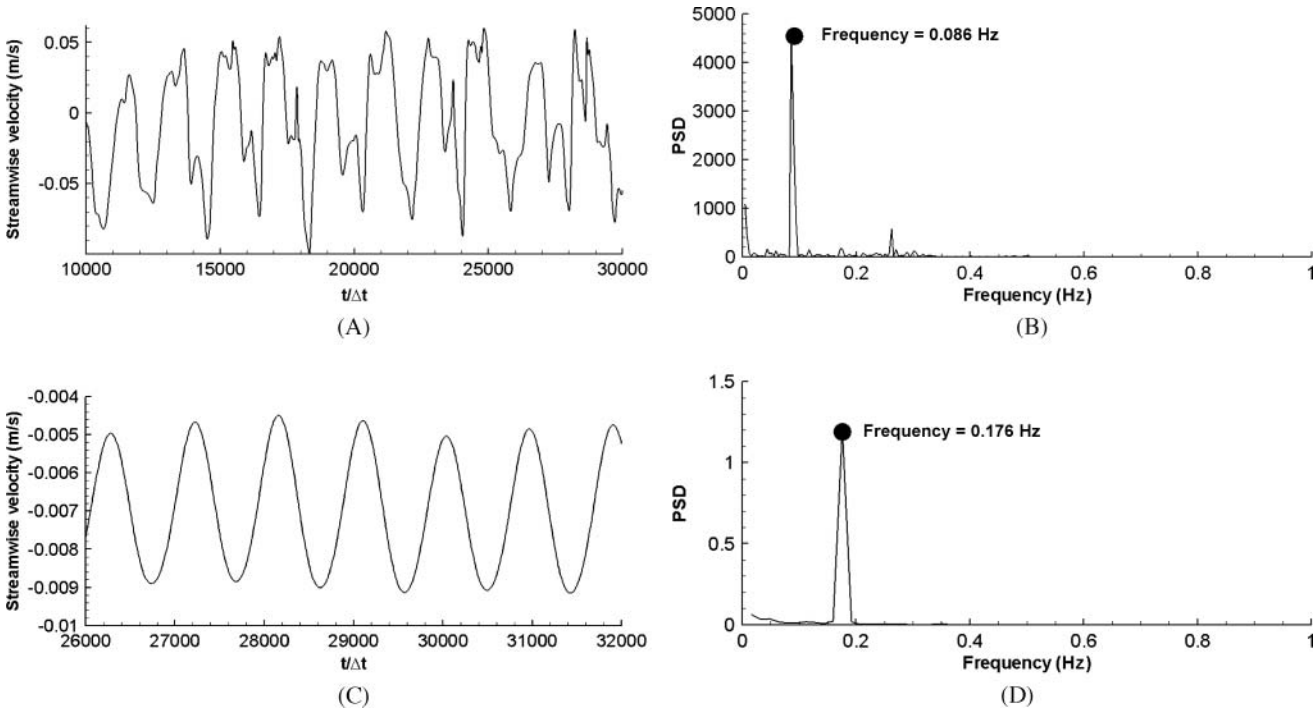

FIGURE 10. Time history of stream-wise velocity and corresponding PSD spectrum at a point (x = 2.4a, y = 6.57a) at Re = 1.0 × 10^3; (A-B) Laminar, (C-D) SST k-ω model.

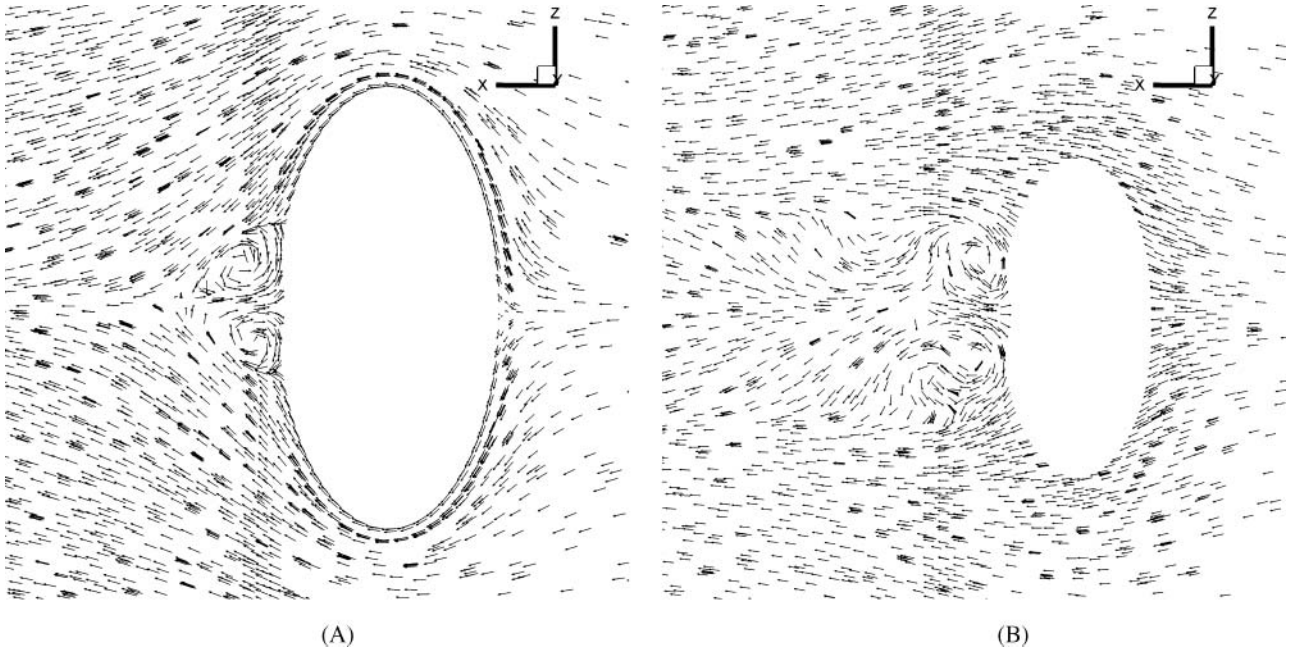

FIGURE 11. Predicted flow field at 5000 time step at (A) waist height (y = 1.17 m), (B) shoulder height (y = 1.37 m).

can leak from the hood or move toward the worker by the mechanism of turbulent diffusion. At low suction rates (low Re), the unsteadiness in the flow can have an enhancing effect on the dispersion of the contaminants inside the hood that in turn may increase the exposure level. The flow patterns can change significantly if the worker stands closer to the hood face.

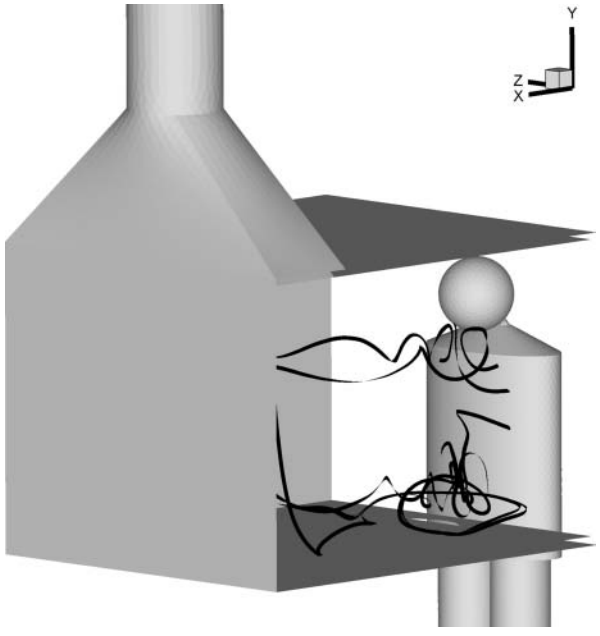

FIGURE 12. Three-dimensional stream-traces at 5000 time step.

Three-Dimensional Case

The predicted vector fields at the waist and shoulder heights around the torso are depicted in Figure 11. It is seen that small, asymmetric and unsteady recirculatory flow structures are present in the wake of the body. These vortices, as in the two-dimensional case, arise from the boundary layer separation around the body. It is also seen from the three-dimensional stream-traces (Figure 12) that other large-scale eddies are present in front of the worker just above the bottom plate of the hood. These eddies are caused mainly by the separation of the flow at the edge of the bottom plate. As the flow withdrawn into the hood flows through the narrow passage between the worker's waist and hood's bottom plate, it accelerates upward and then separates from the bottom plate due to its momentum. The separated flow then forms large eddies tumbling in front of the worker. The size of these eddies depends on the rate of suction. In a more realistic case where buoyancy effect due to worker's body heat is taken into account, larger eddies rising toward the breathing zone are expected.

This complex three-dimensional recirculating flow structures may have significant consequences concerning worker exposure to hazard in fume hoods. Comparison of the predicted flow features reported in experimental studies[5–9] with the predicted flow patterns in the three-dimensional case reveals that the current predictions seem to be accurate. Furthermore, it can be concluded that the SST $k - \omega$ model is capable of predicting anticipated flow dynamics relevant to enclosing fume hoods.

CONCLUSIONS

Two- and three-dimensional analyses of the flow into an enclosing hood obstructed by a worker were performed. The two-dimensional case, originally designed by Dunnett,[1] is a flow around an ellipse into a contraction. Performances of different RANS models, including standard $k-\varepsilon$, RNG $k-\varepsilon$, and SST $k-\omega$, were tested at high, moderate, and low Reynolds numbers. At high Reynolds number (1.0×10^5), all models predicted a steady and symmetric vortex pair in the wake of the worker. In terms of the size of vortices, RNG $k-\varepsilon$ and SST $k-\omega$ model computations yielded remarkably larger vortices. When the Reynolds number was decreased to a moderate level ($\mathrm{Re} = 1.0 \times 10^4$), SST $k-\omega$ model captured some unsteadiness as anticipated from theoretical considerations. On the other hand, the standard and RNG $k-\varepsilon$ models still predicted a steady and symmetric vortex pair in the wake. This might be due to overprediction of the turbulent viscosity that indirectly makes the $k-\varepsilon$ models less responsive to instabilities that lead to vortex shedding. When Reynolds number was decreased even further to 1.0×10^3, SST $k-\omega$ model and laminar flow computations predicted vortex shedding with a single dominant frequency. In contrast to flow around elliptical cylinders immersed in a free-stream, the vortices observed in the present case were confined in a region attached to the cylinder because of suction of the flow into the hood.

Calculations at $\mathrm{Re} = 1.0 \times 10^5$ that are found in the literature did not indicate any flow separation that was captured in the present study, nor did they show any unsteady vortex shedding as opposed to our findings. The present study shows the importance of careful consideration of turbulence models, grid quality, and grid convergence in analyzing the results of CFD application to hood studies.

The flow separation leading to large-scale recirculatory flow structures in more realistic three-dimensional simulations can be considered as indications of complications in the flow. These important flow features induced by the presence of the worker are usually not reported in previous numerical studies. The performance of the SST $k-\omega$ model in capturing the coherent flow structures under the effect of the acceleration into the contraction was found to be promising for further applications of CFD to worker exposure problems.

ACKNOWLEDGMENTS

The authors are grateful to the National Institute of Occupational Safety and Health (NIOSH) for their support on this research (1 R01 OH008165 Enclosing Hood Effectiveness).

REFERENCES

1. **Dunnett, S.J.:** A numerical investigation into the flow field around a worker positioned by an exhaust opening. *Ann. Occup. Hyg. 38(5)*:663–686 (1994).
2. **Flynn, M.R., and C.T. Miller:** Discrete vortex methods for the simulation of boundary layer separation effects on worker exposure. *Ann. Occup. Hyg. 35(1)*:35–50 (1991).
3. **Ingham, D.B., and Y. Yuan:** A mathematical model for the air flow around a worker near a fume cupboard. *Ann. Occup. Hyg. 36(5)*:441–453 (1992).
4. **Delany, N.K., and N.E. Sorenson:** *Low-Speed Drag of Cylinders of Various Shapes* (NACA TN-3038). National Advisory Committee for Aeronautics (NACA), Ames Aeronautical Laboratory, Moffett Field, Calif., November 1953.
5. **Altemose B.A., M.R. Flynn, and J. Sprankle:** Application of a tracer gas challenge with a human subject to investigate factors affecting the performance of laboratory fume hoods. *AIHAJ 59*:321–327 (1998).
6. **Huang, R.F., et al.:** Development and evaluation of an air-curtain fume cabinet with considerations of its aerodynamics. *Ann Occup Hyg. 51(2)*:189–206 (2006).
7. **Ljungqvist, B.:** Air movements—The dispersion of pollutants: Studies with visual illustrative methods. *ASHRAE Trans. 93(1)*:1304–1317 (1987).
8. **Ljungqvist, B.:** Aerodynamic design of fume cupboards. *Saf. Health Pract. 9*:36–40 (1991).
9. **Tseng, L.C., R.F. Huang, C.C. Chen, and C.-P. Chang:** Correlation between airflow patterns and performance of a laboratory fume hood. *J. Occup. Environ. Hyg. 3*:694–706 (2006).
10. **Bennett, J.S., K.G. Crouch, and A.S. Stanley:** Control of wake-induced exposure using an interrupted oscillating jet. *Am. Ind. Hyg. Assoc. J. 64*:24–29 (2003).
11. **Flynn, M.R., and A.D. Eisner:** Verification and validation studies of the time-averaged velocity field in the very near-wake of a finite elliptical cylinder. *Fluid Dyn. Res. 34*:273–288 (2004).
12. **Flynn, M.R., M.-M. Chen, T. Kim, and P. Muthedath:** Computational simulation of worker exposure using a particle trajectory method. *Ann. Occup. Hyg. 39(3)*:277–289 (1995).
13. **George, D., M.R. Flynn, and R. Goodman:** The impact of boundary layer separation on worker exposure. *Appl. Occup. Env. Hyg. 5*:501–509 (1990).
14. **Kulmala, I., A. Saamanen, and S. Enom:** The effect of contaminant source location on worker exposure in the near-wake region. *Ann. Occup. Hyg. 40(5)*: 511–523 (1996).
15. **Chern, M.-J., and W.-Y. Cheng:** Numerical investigation of turbulent diffusion in push-pull and exhaust fume cupboards. *Ann. Occup. Hyg. 51(6)*:517 – 531 (2007).
16. **Hu, P., D.B. Ingham, and X. Wen:** Effect of the location of the exhaust duct, an exterior obstruction and handle on the air flow inside and around a fume cupboard. *Ann. Occup. Hyg. 40(2)*:127–144 (1996).
17. **Lan, N.S., and S. Viswanathan:** Numerical simulation of airflow around a variable volume/constant face velocity fume cupboard. *Am. Ind. Hyg. Assoc. J. 62(3)*:303–312 (2001).
18. **Nicholson, G.P., R.P. Clark, and M.L. Calcina-Goff:** Computational fluid dynamics as a method for assessing fume cupboard performance. *Ann. Occup. Hyg. 44(3)*:203–217 (2000).
19. **Launder, B.E., and D.B. Spalding:** The numerical computation of turbulent flows. *Comput. Method Appl. Mech. Eng. 3*:269–289 (1974).
20. **Richmond-Bryant, J.:** Verification testing in computational fluid dynamics: An example using Reynolds-averaged Navier-Stokes methods for two-dimensional flow in the near wake of a circular cylinder. *Int. J. Num. Meth. 43*:1371–1389 (2003).
21. **Rodi, W.:** Comparison of LES and RANS calculations of the flow around bluff bodies. *J. Wind Eng. Ind. Aerod. 69 – 71*:55–75 (1997).
22. **Yakhot, V., S.A. Orszag, S. Thangam, T.B. Gatski, and Speziale, C.G.:** Development of turbulence models for shear flows by a double expansion technique. *Physics Fluids A. 4(7)*:1510–1520 (1992).
23. **Menter, F.R.:** Two-equation eddy viscosity turbulence models for engineering applications, *AIAA Journal 32(8)*:1598–1605 (1994).
24. **Zhang, Y.:** *Indoor Air Quality Engineering*. Boca Raton, Fla.: CRC Press, LLC. 2005.
25. **Franke, R., and W. Rodi:** Calculation of vortex shedding past a square cylinder with various turbulence models. In *Turbulent Shear Flows 8*, F. Durst et al. (eds.). New York: Springer, 1993. pp. 189–204.